PHYSICAL REVIEW E **75**, 036203 (2007)

Convection patterns in colloidal solutions

B. Huke[1,2], H. Pleiner[2] and M. Lücke[1]
[1] *Institut für Theoretische Physik,Universität des Saarlandes, D-66041 Saarbrücken, Germany*
[2] *Max Planck Insitute for Polymer Research, D–55021 Mainz, Germany*

We investigate the bifurcation properties and pattern selection in Rayleigh–Bénard convecting binary mixtures for parameter combinations that are typical for colloidal fluids using the Galerkin method. In such fluids the typical Lewis numbers and separation ratios differ by orders of magnitude from the values found in molecular mixtures like alcohol/water. We study stationary rolls, square and crossroll patterns for positive separation ratios and traveling waves for negative separation ratios. Results are compared to those for molecular mixtures.

PACS numbers: 47.54.-r 47.20.Bp 47.57.J- DOI: 10.1103/PhysRevE.75.036203

I. INTRODUCTION

A large number of paper deals with the Rayleigh–Bénard convection in binary molecular fluids[1–3]. The rich bifurcation scenarios that emerge from adding the concentration field as new dynamic entity have made this system a popular model system in the field of pattern formation in hydrodynamics.

In binary mixtures, the concentration field couples into the Navier–Stokes equation via the concentration dependent density in the buoyancy force term. Since advection and diffusion alone would lead to an equilibration of the concentration field leaving an effectively one–component system a back–coupling is also necessary. This back–coupling is provided by the Soret effect, the driving of concentration currents by thermal gradients.

The Soret effect can have either a stabilizing or a destabilizing effect on the conductive state depending on whether the Soret generated concentration currents enhance the thermally induced density gradients (positive Soret effect) or diminish them (negative Soret effect). Thus, in the typical case of a positive thermal expansion coefficient, a positive Soret effect means that the lighter component is driven into the direction of higher temperatures and thereby further destabilizes a layer heated from below.

In pure liquids the first convective structure to be found takes the form of stationary rolls, the Bénard rolls. The mixture's bifurcation scenario is much more interesting: For positive Soret effects structures like rolls, squares, and stationary and oscillatory crossrolls have been studied experimentally and theoretically [4–10] at small and moderate heating rates. For negative Soret effect there exist beside rolls also traveling wave structures, and related structures like standing waves, localized traveling waves, and wave fronts [11–18].

In binary gas mixtures the time scale of concentration diffusion is comparable to the heat diffusion and concentration perturbations are easily diffused away. When furthermore the Soret effect is weak the mixture resembles a pure fluid with the same simple bifurcation scenario. Crossrolls and squares for example don't play a role here.

But such patterns can be observed in molecular *liquid* mixtures like alcohol/water. Here the concentration diffusion is much slower, and the time scale is about a factor 100 larger than that of the thermal diffusion. This leads to narrow boundary layers at the plates that must be properly resolved in the simulation. Simulating liquid mixtures therefore requires more numerical resources than simulating pure fluids.

In recent years Rayleigh–Bénard convection in colloidal solution, i. e. binary mixtures of colloidal particles and the carrier liquid has become a focus of interest [19]. Due to the large size of the colloidal particles in the nanometer range the timescale of concentration diffusion is even larger, about 10^4 times the thermal timescale or two orders of magnitude larger than for molecular liquids. Furthermore, colloids were found to have a much stronger Soret effect than molecular mixtures, again by about two or even three orders of magnitude [20]. Numerical simulations of rolls and transient oscillatory structures using a medium–sized Galerkin model were performed in [21, 22].

The goal of this paper is to investigate the bifurcation diagram of binary mixtures for these extreme parameter combinations and to identify the patterns that should be observed in experiments. The paper is organized as follows: In Sec. 2 we will briefly discuss the underlying equations, the Galerkin method that we used for numerical investigations, and the bifurcation scenario as it is known from molecular mixtures. In Sec. 3 we will focus on small amplitude convection and demonstrate the existence of power laws for the critical Rayleigh number and the initial slope of stationary structures. In Sec. 4 we will discuss the full nonlinear convection for positive ψ. We will identify the parameter regions of stable roll patterns, squares, and crossrolls that exist here. In Sec. 5 negative ψ will be discussed, and the bifurcation diagram of rolls and traveling waves. We will summarize our results in Sec. 6.

II. FOUNDATIONS

A. System and basic equations

We consider a horizontal layer of a binary fluid mixture of thickness d that is heated from below in a homogeneous gravitational field, $\mathbf{g} = -g\,\mathbf{e}_z$. A vertical temperature gradient is imposed by fixing the temperature

$$T = T_0 \pm \frac{\Delta T}{2} \;\text{ at }\; z = \mp\frac{d}{2}\,, \tag{2.1}$$

e.g., via highly conducting plates in experiments, i.e., $\Delta T > 0$ throughout this work. We consider the plates to be infinitely extended, rigid, and impermeable. T_0 is the mean temperature of the fluid layer.

In the quiescent conductive reference ground state of the fluid layer the temperature has a linear vertical profile

$$T_{\rm cond}(z) = T_0 - \frac{\Delta T}{d} z\,. \tag{2.2}$$

If there is a Soret effect then this temperature gradient generates a concentration gradient,

$$C_{\rm cond}(z) = C_0 + S_{\rm T} C_0 (1 - C_0) \frac{\Delta T}{d} z\,. \tag{2.3}$$

Here $C = \rho_1/(\rho_1 + \rho_2)$ is the mass concentration of , e.g., the lighter component 1, C_0 is its mean value, and $S_{\rm T}$ is its Soret coefficient. The mass concentration $1 - C = \rho_2/(\rho_1 + \rho_2)$ of the heavier component 2 would then be $1 - C_{\rm cond}(z)$ in the conductive state with $-S_{\rm T}$ being the Soret coefficient of component 2. Thus, e.g., for negative $S_{\rm T}$ the lighter (heavier) component of the mixture is driven into the direction of higher (lower) temperature. For an ordinary thermal expansion coefficient $\alpha > 0$ this means an increase of the density gradient and a further destabilization of a layer heated from below.

Convection is described in terms of the fields of T, C, velocity $\mathbf{u} = (u, v, w)$, total mass density $\rho = \rho_1 + \rho_2$, and pressure P. In the balance equations connecting these fields we scale lengths and positions by d, time by the vertical thermal diffusion time d^2/κ, temperature by $\nu\kappa/\alpha g d^3$, concentration by $\nu\kappa/\beta g d^3$, and pressure by $\rho_0\kappa^2/d^2$. Here ρ_0 is the mean density, κ the thermal diffusivity, ν the kinematic viscosity, and $\alpha = -(1/\rho)\partial\rho/\partial T$ and $\beta = -(1/\rho)\partial\rho/\partial C$ are thermal and solutal expansion coefficients, respectively.

Within the Oberbeck–Boussinesq approximation the transport coefficients κ, ν and the expansion coefficients α, β are taken at the mean values T_0, C_0, P_0 of the thermodynamic variables. Then the balance equations read [2, 23]

$$\nabla\cdot\mathbf{u} = 0 \tag{2.4a}$$

$$(\partial_t + \mathbf{u}\cdot\nabla)\,\mathbf{u} = -\nabla p + \sigma\left[(\theta + c)\,\mathbf{e}_z + \nabla^2\mathbf{u}\right] \tag{2.4b}$$

$$(\partial_t + \mathbf{u}\cdot\nabla)\,\theta = R\,w + \nabla^2\theta \tag{2.4c}$$

$$(\partial_t + \mathbf{u}\cdot\nabla)\,c = R\,\psi\,w + L\left(\nabla^2 c - \psi\,\nabla^2\theta\right)\,. \tag{2.4d}$$

Here θ, c, and p are the reduced deviations of temperature, concentration, and pressure, respectively, from the conductive profiles. The Lewis number L is the ratio of the concentration diffusivity D to the thermal diffusivity κ, therefore measuring the velocity of concentration diffusion. The Prandtl number σ is the ratio of the momentum diffusivity ν and κ:

$$L = \frac{D}{\kappa}\;;\;\sigma = \frac{\nu}{\kappa}\,. \tag{2.5}$$

The Rayleigh number

$$R = \frac{\alpha g d^3 \Delta T}{\nu\kappa} \tag{2.6}$$

measures the thermal driving. The separation ratio

$$\psi = -\frac{\beta}{\alpha} S_{\rm T} C_0 (1 - C_0) = -\frac{\beta}{\alpha}\frac{k_T}{T_0} \tag{2.7a}$$

is proportional to k_T thus incorporating the Soret coupling between temperature and concentration fields. Here $k_T = T_0 C_0 (1 - C_0) S_{\rm T}$ is the so called thermodiffusion ratio. Note that

$$\psi = \frac{\beta}{\alpha}\left(\frac{\Delta C}{\Delta T}\right)_{\rm cond} = \frac{\partial\rho/\partial C}{\partial\rho/\partial T}\left(\frac{\Delta C}{\Delta T}\right)_{\rm cond} \tag{2.7b}$$

is the solutally induced vertical density change divided by the thermally induced density change, say, in the conductive state. The value of ψ does not depend on the component chosen to define the concentration. If one defines C as the concentration of the heavier component, the more intuitive choice in the case of colloids like ferrofluids, instead of the lighter component, as it is traditionally done for molecular mixtures, both β and S_T change sign, such that the products βS_T and βk_T remain unchanged.

Typically $\sigma = \mathcal{O}(10)$ in liquid mixtures, and compared to the other parameters the exact value has only a weak influence on the convection for $\sigma \gg 1$. We will always use $\sigma = 10$ in our calculations. In liquid molecular mixtures a typical value for the Lewis number is 0.01, whereas in colloids L can easily reach values as low as 10^{-4}. The much slower diffusion in colloids is a consequence of the large size of colloidal particles compared to small molecules making them less susceptible to Brownian motion. ψ finally is generally much larger in colloids than in molecular mixtures. Values of $\mathcal{O}(10)$ and larger have been found [20]. In comparison, in alcohol/water one finds values of ψ in the range between -0.5 and 0.5 depending on the mean concentration and temperature. The large values for ψ have also been explained as being caused by the large particle size [24].

For the velocity field we impose realistic no slip boundary conditions $\mathbf{u} = 0$ at the plates. The velocity field is written as

$$\mathbf{u} = \nabla\times\nabla\times\Phi\mathbf{e}_z + \nabla\times\Psi\mathbf{e}_z\;\;, \tag{2.8}$$

what automatically fulfills (2.4a).

Equations for the potentials Ψ and Φ can be derived by taking the third component of the rotated and double–rotated Navier–Stokes equation (2.4b). This also eliminates the pressure term. The boundary conditions translate to $\Phi(z) = \partial_z\Phi(z) = \Psi(z) = 0$ at $z = \pm 1/2$. Since the plates are kept at constant temperature it is $\theta(z = \pm 1/2) = 0$. At the impermeable plates the vertical concentration current vanishes, i.e., $\partial_z(c - \psi\theta) = 0$ there. Thus, we use instead of c the combined field

$$\zeta = c - \psi\theta\,. \tag{2.9}$$

An equation for ζ can be easily derived from (2.4c) and (2.4d).

B. Numerical methods

To find the convective solutions and to test their stability we used the Galerkin method. For the *nonpropagating* structures the fields $X = \Phi, \theta, \zeta$ are expanded into orthogonal modes in the following way:

$$X(x, y, z; t) = \sum_{lmn} X_{lmn}(t)\cos(lkx)\cos(mky)f_n^X(z)\ . \tag{2.10}$$

For Ψ the lateral cos expansion must be replaced by an expansion in sin functions. The f_n^X form a complete orthogonal set of functions in z that fulfills the boundary conditions for the field X. We use Chandrasekhar functions [25] for Φ and otherwise trigonometric functions with a growing number of nodes. The lateral wave number k of the patterns enters into the calculation as a fifth parameter.

The expansion is cut off at sufficiently high indices l, m, n. We took all θ and ζ–modes into account for which $l + m + n < N$ with $N = 60$ for two–dimensional structures and $N = 28$ for three–dimensional structures. Φ and Ψ can in general be approximated well with less modes: here we used $N = 30$ and $N = 14$, respectively.

Inserting the ansatz into the basic equations and projecting them onto the orthogonal modes results in a nonlinear system of coupled ordinary differential equations of first order in time for the $X_{lmn}(t)$. Those stationary solutions of this system that were of interest were obtained using the Newton–Raphson algorithm. In addition stability analyses of these stationary states were done: after linearizing the equations around the fixed points the resulting eigenvalue problem was solved numerically.

Three different nonpropagating structures were investigated: rolls, squares, and crossrolls. All of them fulfill the mirror–glide symmetry

$$X(x, y, z) = \pm X(x + \pi/k, y + \pi/k, -z) \tag{2.11}$$

which allows to set half of the modes to zero. Furthermore, for two–dimensional structures like stationary rolls, say, with axes oriented in y-direction all amplitudes X_{lmn} with $m \neq 0$ can be set to zero. The Ψ field is not needed for these structures at all. Squares have a $x \leftrightarrow y$ symmetry such that $X_{lmn} = \pm X_{mln}$. Here the minus sign holds for Ψ. The third structure, the crossrolls exhibit no additional symmetry.

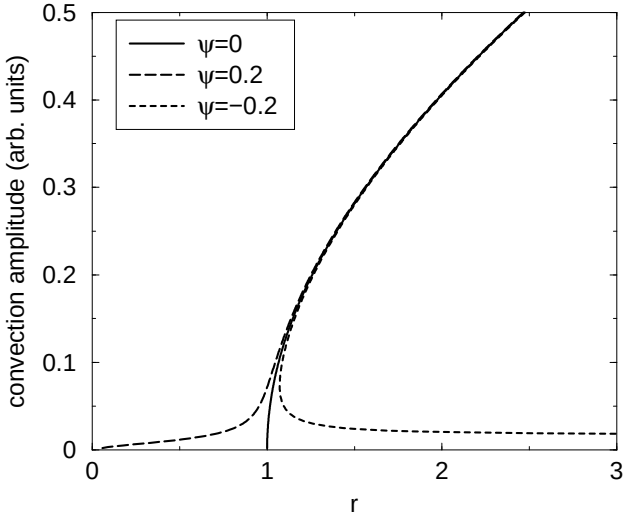

FIG. 1: Bifurcation diagram of convection amplitude versus r for stationary rolls with wave number $k = k_c^0$ in pure fluids ($\psi = 0$) and mixtures with negative and positive Soret coefficients, $\sigma = 10$, and $L = 0.01$.

As a fourth structure traveling waves (TWs) of laterally propagating rolls are discussed in this paper. After transient relaxation processes have died out TWs move with constant amplitude and constant phase velocity ω/k, say, in x-direction. Thus, they can be described by

$$X(x, y, z; t) = \sum_{l,n} X_{l0n}e^{il(kx-\omega t)}f_n^X(z) + c.c.\ . \tag{2.12}$$

But additionally, a lateral velocity component

$$u^{MF}(z) = \sum_n u_n^{MF}f_n^{MF}(z) \tag{2.13}$$

is needed to describe a mean flow. This simple form of the TW's time dependence allows to apply the Galerkin method. Here, however, the amplitudes X_{l0n} are complex for $l \neq 0$. Only one amplitude, e.g., Φ_{101} can be assumed to be real thereby fixing the phase. Instead of the imaginary part, the TW frequency ω enters as a new unknown.

C. Bifurcation of stationary rolls

In this section we briefly review the bifurcation properties of stationary rolls in molecular fluids. In pure fluids ($\psi = 0$) convection starts at a critical Rayleigh number $R_c(\psi = 0) \approx 1708$. The wave number of the critical mode is $k_c^0 \approx 3.116$ [26]. The first pattern to appear takes

the form of parallel convection rolls with alternating direction of rotation, known as Bénard rolls that bifurcate forward out of the conductive state [27]. Similar roll patterns also play a role in binary mixtures for both positive and negative ψ.

Fig. 1 shows the bifurcation diagrams of stationary rolls for $L = 0.01$, $k = k_c^0$, and three different ψ. We have plotted the leading velocity amplitude versus the reduced Rayleigh number

$$r = R/R_c(\psi = 0)\,. \tag{2.14}$$

We use r throughout this paper as a control parameter. For the pure fluid the shape of the curve can be well approximated in the r-range of Fig. 1 by its initial behavior $\sim \sqrt{r-1}$ close to onset.

Rolls bifurcate for $\psi = 0.2$ at much lower r out of the conductive ground state than in pure fluids because for positive ψ the Soret induced solutal contribution to the local density enhances the buoyancy and thus destabilizes the quiescent fluid. For the parameters of Fig. 1 two different regimes can be clearly distinguished. In the so–called Soret region at $r < 1$ the convection amplitude is very low before it curves upwards at $r \approx 1$. Thereafter, the stronger convective flow leads to a better mixing such that at $r > 1$, i.e., in the Rayleigh region the bifurcation behavior becomes very similar to that of the pure fluid.

On the other hand, for negative ψ the ground state is stabilized and the bifurcation is backwards except for separation ratios very close to zero. In fact, for $\psi = -0.2$ the stabilization is so strong that stationary rolls cannot grow out of the quiescent fluid starting from infinitesimal perturbations: the roll bifurcation threshold has moved already up to $r = \infty$, the solution branch for stationary rolls in Fig. 1 is detached from the quiescent state, and it requires a *finite* initial amplitude to start the growth of stationary rolls. As long as only non oscillatory perturbations are considered, i.e., if one suppresses in particular the phase oscillations that lead to TWs the upper branch of the short dashed curve in Fig. 1 would be stable coexisting with the stable ground state while the lower branch to the right of the saddle node bifurcation is amplitude unstable. As for $\psi = 0.2$ the mixture convection resembles very closely the pure fluid convection when the convective mixing becomes strong enough.

III. SMALL-AMPLITUDE STATIONARY CONVECTION FOR $\psi > 0$

Before convection in colloidal solutions at moderate and high amplitudes is discussed we address briefly convection with small amplitudes close to onset. Note that small-amplitude convection is typically unstable for $\psi < 0$ — except when ψ is very close to zero — because of the backwards bifurcation behavior of stationary rolls as well as of TWs. We therefore restrict the discussion in this section to positive separation ratios.

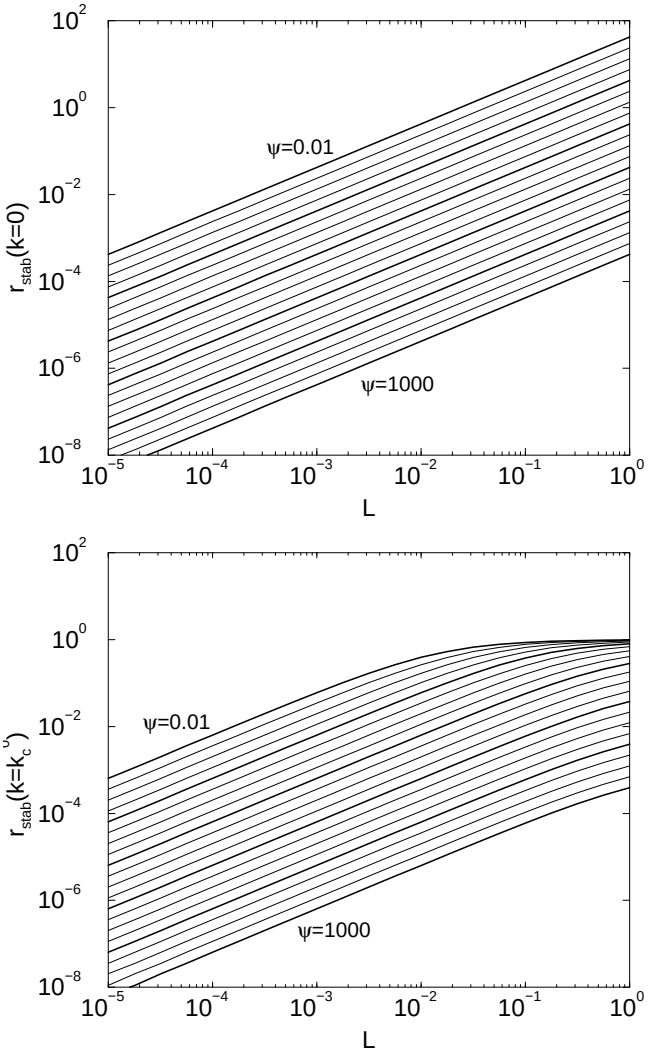

FIG. 2: Reduced stability thresholds of the conductive state, $r_{\rm stab}(k, \psi, L)$, against non oscillatory convection with wave numbers $k = 0$ (top) and $k = k_c^0$ (bottom) versus L. Between thick lines ψ changes by a factor of 10.

A. Bifurcation thresholds

The critical wave number at onset of convection is $k_c = 0$ when $\psi \geq \psi_\infty = 131L/(34 - 131L)$ [30]. Thus, for $L \ll 1$ one has $\psi_\infty \approx 3.85L$. For typical molecular liquid mixtures and even more so for colloidal liquids the convection at onset seems to form a single cell of the size of the container [31]. With increasing Rayleigh numbers, on the other hand, the observed wave number has been found to quickly approach values that are more similar to the critical one, k_c^0, of pure fluids [8, 32].

In Fig. 2 the reduced stability thresholds of conduction against bifurcation of stationary rolls, $r_{\rm stab}(k, \psi, L)$, are shown as functions of L for several ψ-values for two fixed wave numbers: $k = 0$ and $k = k_c^0$ as a representative example for a finite wave number. Note that $r_{\rm stab}$ does not depend on σ. The plots show that $r_{\rm stab}$ follows a

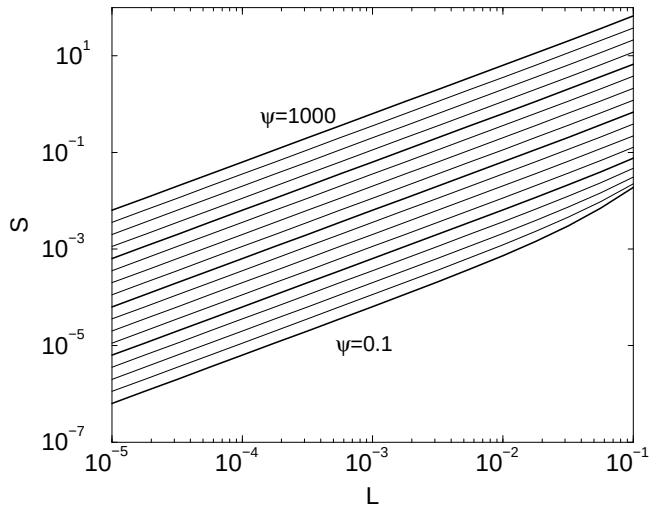

FIG. 3: Initial slope of the Nusselt number as a function of L for $\sigma = 10$, $k = k_c^0$. Between thick lines ψ changes by a factor of 10.

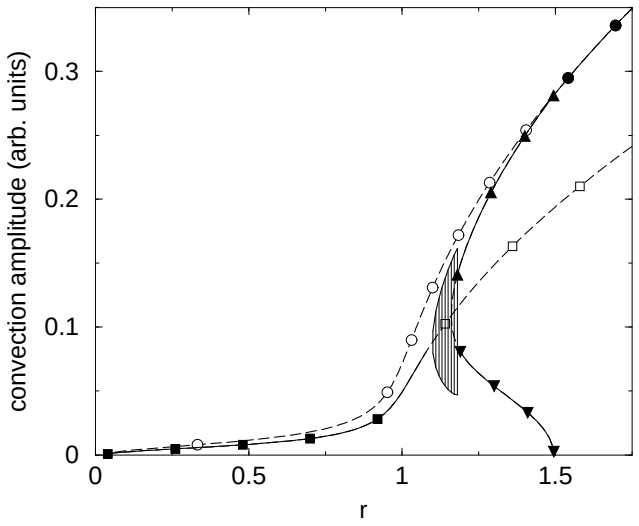

FIG. 4: Bifurcation diagram of rolls (circles), squares (squares), stationary crossrolls (triangles), and oscillatory crossrolls (striped area) for $L = 0.01$, $k = k_c^0$, and $\psi = 0.2$. Lines with circles, squares, and upwards pointing triangles denote x-roll amplitudes. Downwards pointing triangles refer to y-roll amplitudes of the stationary crossroll solution. Vertical lines indicate x- and y-rolls amplitude variations of oscillatory crossrolls. Stable (unstable) stationary structures are represented by solid (dashed) lines and solid (open) symbols.

power law in L and ψ of the form

$$r_{\rm stab}(k,\psi,L) = h(k)\frac{L}{\psi} \tag{3.1}$$

with a prefunction $h(k)$ that takes the values $h(0) \approx 0.42$ and $h(k_c^0) \approx 0.63$. For $k = k_c^0$ there are deviations from this power law behavior at large L and small ψ that are, however, not relevant here. Note that the threshold $r_{\rm stab}$ is practically zero for colloidal parameters.

The power law for finite k can also be derived analytically. The linear stability analysis of the ground state [30] leads to a relation between $r_{\rm stab}$, k, and the other parameters of the form

$$f(k,\tilde{r}_{\rm stab}) = p\; g(k,\tilde{r}_{\rm stab}) \quad . \tag{3.2}$$

Here $p = \psi/[L(1+\psi)]$ and

$$\tilde{r}_{\rm stab} = (1+\psi+\psi/L)\, r_{\rm stab} \quad . \tag{3.3}$$

In the limit $L \to 0$, $\psi \to \infty$, p approaches infinity. In order to fulfill (3.2), $\tilde{r}_{\rm stab}$ must approach a value $\tilde{r}_{\rm stab,0}$ in this limit, such that $g(k,\tilde{r}_{\rm stab,0}) = 0$. It is then $r_{\rm stab} \approx \tilde{r}_{\rm stab,0}\, L/\psi = {\rm const}\; L/\psi$.

For $k = 0$ a more careful analysis is necessary since then both, $f(k,\tilde{r}_{\rm stab})$ and $g(k,\tilde{r}_{\rm stab})$ go to zero for $k \to 0$. It is known that the power law $r_{\rm stab} = h(k)L/\psi$ holds for arbitrary ψ and L in this case with an exact value of $h(0) = 720/R_c^0$ [30].

B. Initial slope of the Nusselt number $N(r)$

An important nonlinear quantity that characterizes convection with small amplitudes close to onset is the initial slope

$$S = \frac{\partial N}{\partial r} \qquad \text{at } r = r_{\rm stab} \tag{3.4}$$

of the growth of the Nusselt number N with r. Fig. 3 shows the variation of S with L for different ψ and fixed $k = k_c^0$ for the case of stationary roll convection. Contrary to the convective threshold $r_{\rm stab}$ the initial slope S does depend on σ but the dependence on this parameter is weak for $\sigma \gg 1$.

Square patterns while having the same bifurcation threshold $r_{\rm stab}$ as roll patterns have a slightly different Nusselt number. But this difference is too small to be seen in Fig. 3. For $L < 0.01$ the ratio of the corresponding initial slopes is about constant, $S_{\rm rolls}/S_{\rm squares} \approx 0.980$, and then it increases with growing L to ≈ 0.983 at $L = 0.1$. The ratio depends very weakly on ψ.

Except for large L and small ψ the initial slopes S of the Nusselt numbers obey also a power law, namely $S \sim L\psi$. This result too can be reasonably well explained within a few–mode model. From [33] one can derive an expression

$$S = \frac{242}{387}\psi L \tag{3.5}$$

in the limit $L \to 0$, where $242/387 = 0.625...$ agrees well with the value of 0.631 we found when fitting to the data at small L.

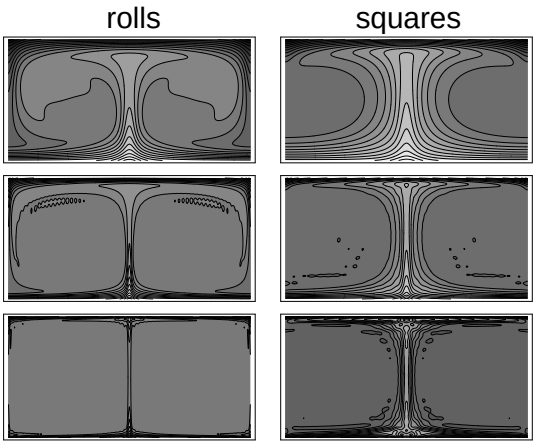

FIG. 5: Concentration field of convective roll and square states in the vertical $x-z$-plane at $y=0$ that conains the upflow maximum and that extends laterally over one wave length in x-direction. Parameters are $\sigma=10$, $k=\pi$, $r=1$, and from top to bottom: $(L,\psi)=(0.01,\,0.1)$, $(0.001,\,1)$, $(0.0001,\,10)$. A lighter (darker) shade of grey denotes a higher concentration of the lighter (heavier) component. Note the pronounced boundary layer structure for small L and large ψ.

IV. ROLLS, SQUARES, AND CROSSROLLS FOR $\psi > 0$

A. Bifurcation and stability scenario

At positive ψ rolls are stable close to onset only if L is sufficiently large and ψ is small [34]. In this case the concentration differences that are generated by the Soret effect are weak. Moreover, they are diffused away efficiently. Thus, the fluid still behaves qualitatively like a pure fluid even when advection is small, i.e., even for small convection amplitudes. For smaller L or larger ψ, however, rolls turn out to be unstable near onset against a square pattern that emerges at the same bifurcation threshold. The square structures can be thought of as being a superposition of two equal strength perpendicular roll sets that we shall call x-rolls and y-rolls for short. The x- and y-roll convection amplitude of the squares is smaller than the amplitude of a pure roll state at the same control parameters.

At higher Rayleigh numbers when the mixing is stronger rolls become stable again. In between, a third stationary structure exists, the crossrolls which transfer stability from the squares to the rolls. Crossrolls can be thought to consist of two perpendicular roll sets like squares, but with different amplitudes.

A bifurcation diagram of squares, crossrolls, and rolls is shown in Fig. 4. The order parameter is the amplitude of one of the roll sets, say, the rolls in x-direction. Near the bifurcation point to the square branch the crossroll amplitudes are similar, but then the difference grows. There are two different symmetry degenerate crossroll states: In one case the x-component is the dominant set and the crossroll structure ends on the solution branch of x-rolls. In the other case the y-component is stronger and the x-component becomes smaller until it vanishes and the crossroll branch ends in the y-roll branch.

There is a fourth structure that is displayed in Fig. 4, the oscillatory crossrolls. They exist only at small L but still at parameters that are easily realizable with alcohol-water mixtures. The oscillatory crossrolls bifurcate from the square branch before the stationary crossroll branch appears. They end up on the latter in a complex entrainment process [9]. In the oscillatory crossrolls x- and y-roll amplitudes oscillate in counterphase such that one of them is alternatingly dominant with squares appearing twice in such a cycle. The striped area in Fig. 4 is bounded by the maximal and minimal amplitudes of x- and y-rolls during one oscillation period. Note that the minimal amplitudes remain well above zero.

B. Concentration boundary layers

We already have mentioned that the very slow solutal diffusion together with a very strong Soret effect can be expected to generate very narrow boundary layers. This boundary layer structure becomes apparent in Fig. 5. The plots show the concentration field of rolls and squares in the vertical plane at $y=0$ that conains the maximum upflow and that extends over one lateral wave length in x-direction. In the two top plots $(L,\psi)=(0.01,0.1)$ is typical for molecular liquids. In the two bottom plots values of $(L,\psi)=(10^{-4},10)$ were chosen that are typical for colloids.

In all shown cases many modes contribute significantly to the concentration field giving rise to a very anharmonic profile. In contast to that, the temperature field at this point can still be very well described by two (four) modes in the case of rolls (squares). For the colloidal parameters the concentration distribution is practically homogeneous except directly at the plates and between the rolls where concentration is advectively transported downwards (at the left and right sides or the plot) or upwards (in the center).

The boundary layers of the square structures are in general broader than those of the rolls as Fig. 5 shows. This is fortunate, since the simulation of three–dimensional structures requires a priori more modes than in the two–dimensional case. But the less pronounced boundary layers allows to reduce the resolution, i. e., the number of modes, especially since squares exist as stable structures only at smaller r where the boundary layers are broader in any case.

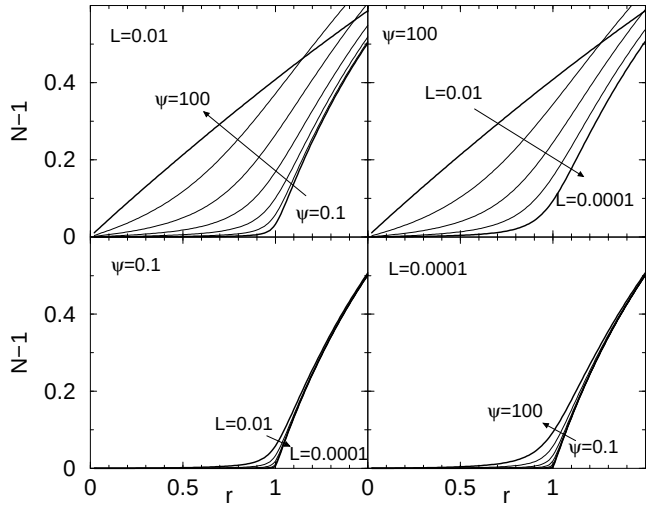

FIG. 6: Nusselt number versus r for $\sigma = 10$, $k = k_c^0$, and several (L, ψ)–combinations. The parameter that is varied changes by a factor of $\sqrt{10}$ between the curves in each plot.

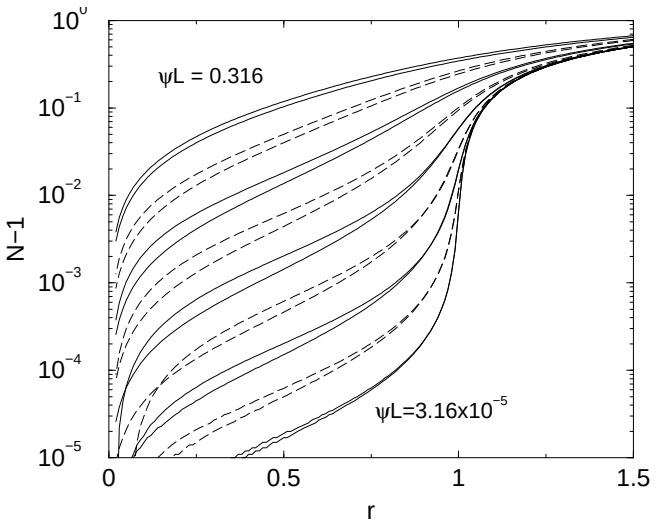

FIG. 7: Nusselt number versus r for the parameter combinations of Fig. 6, i.e., $L = 10^{-2-n/2}$ $(n = 0, ..., 4)$ combined with $\psi = 10^{-1+m/2}$ $(m = 0, ..., 6)$ without the extreme combinations $(L, \psi) = (0.01, 100)$ and $(0.0001, 0.1)$. For a pair of curves that are alternatingly shown by dashed and solid lines the product $L\psi$ is the same. From pair to pair it changes by a factor of $\sqrt{10} = 3.16$.

C. Changes in the bifurcation behavior with varying ψ, L

The bifurcation diagrams of rolls for $\sigma = 10$, $k = k_c^0$, and several (L, ψ)–combinations are shown in Fig. 6. Again, the Nusselt number was chosen as order parameter. Since the Nusselt numbers of squares differ only very slightly from those of rolls — not only near onset but also at higher r — the former are not shown here. The same holds true for the stationary crossrolls in their r-interval of existence. The closeness of the $N(r)$ curves for the different convection structures is somewhat unfortunate for experiments with intransparent liquids that do not allow a direct visual observation of the convection patterns: investigating the bifurcation scenario of the aforementioned stationary convection structures by Nusselt number measurements only would be a real experimental challenge. Odenbach [35] followed a different approach, measuring the small temperature variations at the plates to discriminate between square and roll patterns in convecting ferrofluids.

When the product $L\psi$ is small, the transition between Soret– and Rayleigh regime is very sharp and the amplitudes in the Rayleigh region agree well with those of the pure fluid. This is not the case for large $L\psi$ where the transition is rather smooth and where in the Rayleigh region the curves of $N(r)$ show substantial deviations from the pure fluid Nusselt number. The reason for these deviations from pure fluid convection is that temperature gradients generate for large ψ strong concentration gradients that are not adjectively mixed away easily when the concentration diffusion is fast, i. e., when L is also large.

In Fig. 7 all curves of Fig. 6 except for the limiting cases $[(L, \psi) = (0.01, 100)$ and $(L, \psi) = (0.0001, 0.1)]$ of largest and smallest $L\psi$ are plotted again r in one single logarithmic plot. In this way the variation of N with r in the Soret region becomes better visible. The curves are grouped in solid and dashed pairs that share the same value of $L\psi$. From pair to pair it changes by a factor of $\sqrt{10}$. This demonstrates that changing L and ψ while keeping its product constant does indeed have only a minor influence on $N(r)$. Thus, in colloids the effects of the large ψ and the small L tend to compensate each other, resulting in bifurcation diagrams that are very similar to those of molecular liquid mixtures with similar values of the product $L\psi$.

D. Phase diagrams

Fig. 8 shows an overview of our results concerning the bifurcation properties at positive ψ in the form of phase diagrams in the $r - \psi$-plane. For four different small values of L and a broad range of ψ we calculated the r-values of the bifurcation thresholds: (i) from squares to oscillatory crossrolls, (ii) from squares to stationary crossrolls, and (iii) from rolls to stationary crossrolls.

Above the dark gray regions in the plots of Fig. 8 rolls are the stable structures. They lose their stability at the upper boundary of the gray regions where the stationary crossroll branch meets the roll branch. Squares, on the other hand, are stable below the light gray area. The lower boundary of the light gray area marks the r-values where oscillatory perturbations become supercritical and where oscillatory crossrolls emerge. The boundary between the light gray and the dark gray area finally is the location where squares lose stability also against sta-

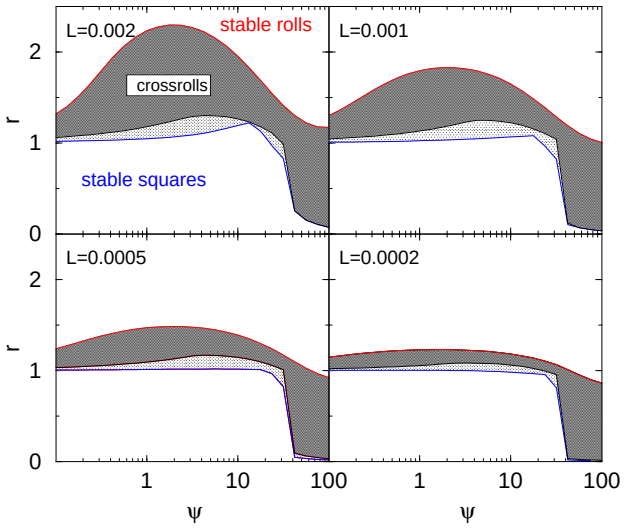

FIG. 8: (color online) r–ψ–phase diagrams for squares, oscillatory crossrolls, stationary crossrolls, and rolls for $k = k_c^0$, $\sigma = 10$, and four different L. Rolls are stable in the upper region, squares in the lower. Crossrolls exist in the gray regions. See text for further details.

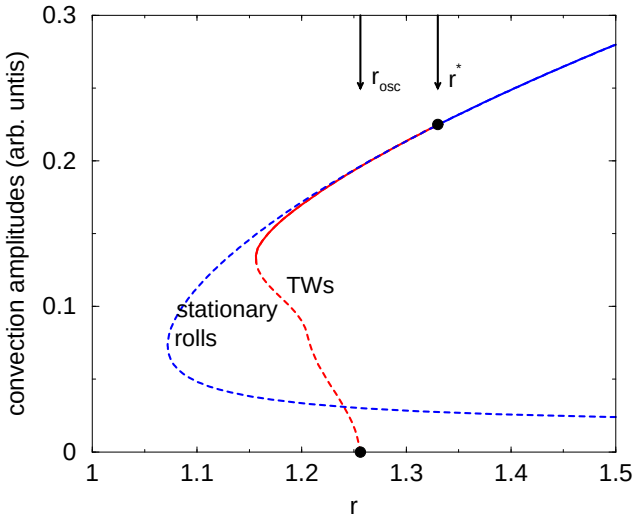

FIG. 9: (color online) Bifurcation diagram of stationary rolls and traveling waves (TWs) for $L = 0.01$, $k = k_c^0$, and $\psi = -0.2$. Stable (unstable) structures are represented by solid (dashed) lines.

tionary perturbations and where the stationary crossroll solution bifurcates out of the square solution.

For colloid parameters our nonlinear results for the crossroll fixed points become unreliable at higher r — there even in the largest 3D models that we used the crossroll solution branch did not end on the roll solution branch anymore. However, this is a numerical artifact: we verified with more extensive linear stability analyses of the roll solution branch that the bifurcation from rolls to stationary crossrolls still exists. We therefore did not try to calculate the position of the fourth important bifurcation point in the bifurcation scenario for positive ψ, i. e., the point where stationary crossrolls lose stability against oscillatory crossrolls. Oscillatory crossrolls can be expected to exist not only in the light gray area, but also in the lower part of the dark gray area. Stationary crossrolls, on the other hand, can be expected to be stable only in the upper parts of the dark gray regions.

Square patterns lose their stability at about $r = 1$ as long as $\psi \leq 30$. For larger ψ this changes very abruptly, reducing the stability region of squares to a very small stripe directly above onset. The first instability of squares is then still oscillatory but stationary instabilities set in very close by. This happens at about the same position also in Galerkin expansions that take into account fewer modes than the ones used in obtaining Fig. 8. We therefore consider it as unlikely that this feature is an artifact coming from a premature mode truncation in the Galerkin expansion.

Roll convection gains stability earlier when L is small: for $L = 0.0002$ the region of stability reaches down almost to $r = 1$, leaving for $\psi \leq 30$ only a small r-interval where crossrolls exist. Both, large and small ψ seem to favor roll convection. For fixed L its stability boundary marking the bifurcation threshold to crossrolls has a maximum in r at about $\psi = 2$.

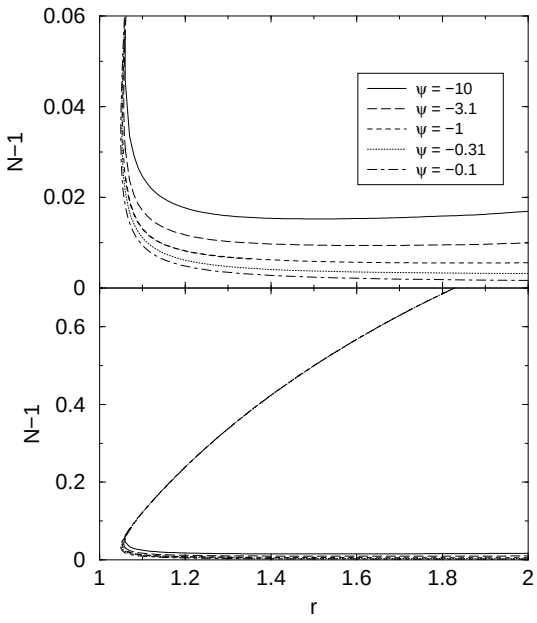

FIG. 10: Bifurcation diagram of Nusselt number versus r of stationary rolls for $\sigma = 10$, $k = k_c^0$, and different negative ψ such that $|L\psi| = 10^{-4}$. Top plot is a magnified part of the bottom plot.

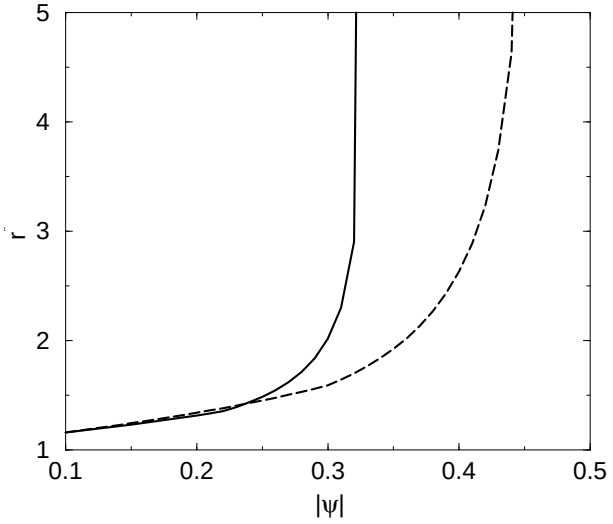

FIG. 11: Endpoint r^* of the TW solution branch for $\sigma = 10$ and $k = k_c^0$ as a function of ψ for fixed $L = 0.01$ (dashed line) and for $L\psi = -10^{-4}$ (solid line).

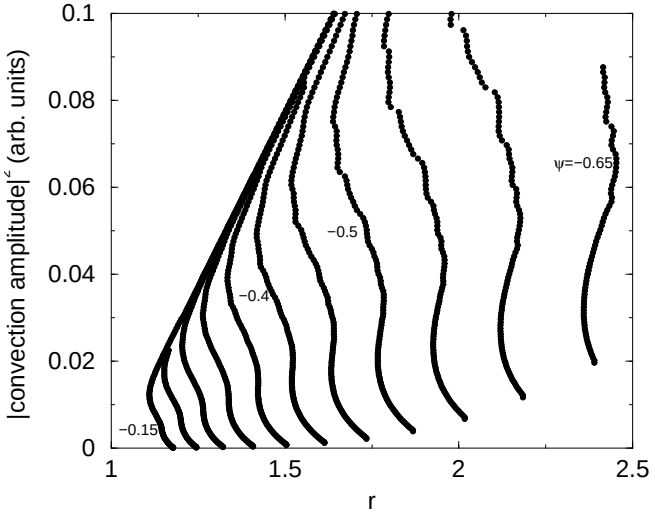

FIG. 12: Bifurcation diagrams of squared TW convection amplitudes versus r for $\sigma = 10$, $k = k_c^0$, $L\psi = -10^{-4}$, and several values of ψ between -0.15 and -0.65.

V. TW AND STATIONARY ROLL CONVECTION FOR $\psi < 0$

For negative separation ratios one can observe not only stationary but also oscillating convection rolls. The latter appear in the transient growth at supercritical heating, in spatially extended relaxed nonlinear TW and standing wave (SW) solutions that branch out of the conductive state at a common Hopf bifurcation threshold r_{osc}, in spatially localized traveling wave (LTW) states, and in various types of fronts. TW and LTW convection has been studied experimentally and theoretically for some time [1, 14, 15, 36–44]. Nonlinear relaxed SW solutions [16, 17] and freely propagating convection fronts [18] that connect subcritically bifurcating TWs with the *stable* quiescent fluid were obtained only recently.

Here we investigate the competition between extended stationary and TW convection as it can be observed in experiments in narrow rectangular and annular channels which enforce the roll axes to be oriented perpendicular to the long sidewalls. These stuctures can efficiently be described in the two dimensional vertical $x - z$ cross section in the middle of the channel perpendicular to the roll axes ignoring variations in axis direction. Furthermore, these convection structures have relevant phase gradients only in x-direction thus causing effectively one dimensional patterns.

Fig. 9 shows a bifurcation diagram for both structures in the case of a typical molecular liquid mixture. The oscillatory threshold r_{osc} precedes the bifurcation to stationary rolls at r_{stat}. In fact for the parameters $\psi = -0.2$, $L = 0.01$ of Fig. 9 the bifurcation threshold for stationary rolls has already moved up to ∞: r_{stat} increases monotonously from 1 at $\psi = 0$ to ∞ at $\psi = -L/(1 + L)$ [30].

Both convection structures bifurcate backwards. The TW phase velocity decreases with growing amplitude until the TW solution branch meets with zero phase velocity the upper stationary roll branch in Fig. 9 at some reduced Rayleigh number r^*. Only after this bifurcation point the stationary solution is stable. For $L = 0.01$ the heating rate r^* grows with increasing $|\psi|$ and finally diverges for $\psi \approx -0.45$ such that the whole stationary branch becomes unstable (see Fig. 11 below).

At $\psi \lesssim -1$ the stabilizing effect of the concentration gradient overcompensates the destabilizing effect of the thermal gradient. For such a strong negative separation ratio no oscillatory bifurcation threshold $r_{osc} < \infty$ exists for any parameter combination. Then the ground state is linearly stable and neither stationary nor TW roll solutions with *arbitrarily small* convection amplitudes exist anymore. However, when convection is strong enough it can advectively mix, reduce, and equilibrate the concentration field and thereby selfconsistently sustain itself in an environment that is mixed by the convective flow. Therefore, the stationary and oscillatory roll branches still exist but without connection to the ground state. As in the case of $\psi > 0$ a small L is required to allow the advective mixing to be effective when $|\psi|$ is large.

This explains qualitatively that, e.g., the stationary roll branches depend only very weakly on the product $L\psi$ as the lower plot of Fig. 10 demonstrates. There the Nusselt number is shown for $|L\psi| = 10^{-4}$ and for separation ratios that span over two orders of magnitude. There is however some variation in the lower branch as can be seen in the upper plot of Fig. 10 where this branch in shown again on an expanded scale.

On the other hand, the behavior is quite different when ψ is increased while L is kept fixed: Then the stationary solution branches are shifted towards larger r and, e. g., for $L = 0.01$ and $\psi = -9$ the stationary saddle has

already moved up to $r \approx 3$.

One might expect that the very weak $L\psi$-dependence of the variation of the upper stationary branch with r also extends to its stability. But this is not the case as Fig. 11 shows: r^* as a function of ψ does not only diverge for a fixed L, but also when the product $L\psi$ is kept constant. In the latter case the point of divergence is reached even earlier.

Not only r^* but the TW–branch as a whole is shifted towards larger r with growing $|\psi|$. This is shown in Fig. 12, again for constant $L\psi = -10^{-4}$. For a fixed $L = 0.01$ this behavior is qualitatively the same [45]. We should like to mention that for small L the convergence properties of our Newton–Raphson algorithm for determining the TW-solutions become poor. This is reflected by the visible jitter in some of the curves of Fig. 12.

We can conclude that neither the convection in form of stationary rolls nor *TW*–convection which are the important forms of convection in molecular mixtures for negative separation ratios play a role in colloidal mixtures with large negative ψ. Already at $\psi > -1$ the roll branch has lost its stability and a TW–branch does not even exist at moderate r anymore.

VI. CONCLUSION

We have studied the bifurcation scenarios in the Rayleigh–Bénard system at very small L and large $|\psi|$ as typical for colloidal fluids using the Galerkin method and compared the results to those for parameter combinations more typical to molecular liquid mixtures.

In molecular liquid mixtures with a positive separation ratio convection sets in at very small Rayleigh numbers compared to the critical value of $R_c^0 \approx 1708$ in pure fluids. In colloids the onset happens at even smaller R. We found a power law $R_{\rm stab} \sim L/\psi$ to hold as predicted by the semi–analytic linear stability analysis.

The initial slope of roll and square structures defined as the onset slope of the Nusselt number on the other hand was found to be proportional to $L\psi$. This product also approximately determines the whole $N(r)$ curve for both positive and negative ψ such that the roll branches of molecular liquids and colloids look very similar.

For colloids with positive separation ratios we found essentially the same sequence of stable structures as for molecular liquids with squares being stable at small r, rolls being stable at large r, and oscillatory and stationary crossroll patterns in between. For small L and the r–intervall where crossrolls exist is very small as long as $\psi < 30$. Squares and rolls are stable in practically the whole Soret region $r < 1$ and Rayleigh region $r > 1$, respectively. At larger ψ however square patterns are strongly disfavored and instable against crossroll perturbations in the Soret region except very close to the onset.

For negative separation ratios and Lewis numbers typical for colloidal solutions neither stable roll nor TW–convection is possible. The TW–branch is shifted towards higher r with growing $|\psi|$ such that already for $|\psi| = \mathcal{O}(1)$ TW–convection is not possible anymore at moderate r. The roll branch does not move with growing $|\psi|$ when $L\psi$ is kept constant, but loses rapidly its stability as R^*, the Rayleigh number of the bifurcation from TWs to rolls diverges.

Acknowledgment

This work was supported by the Deutsche Forschungsgemeinschaft.

[1] M. C. Cross and P. C. Hohenberg, Rev. Mod. Phys. **65**, 851 (1993)
[2] J. K. Platten, J. C. Legros: *Convection in Liquids.* (Springer, New York 1984)
[3] M. Lücke, W. Barten, P. Büchel, C. Fütterer, St. Hollinger, Ch. Jung: 'Pattern formation in binary fluid convection and in systems with throughflow'. In: *Evolution of spontaneous structures in continuous systems* ed. by F. H. Busse, S. C. Müller. Lecture Notes in Physics **55**, 127. (Springer, Berlin, Heidelberg 1998)
[4] P. Le Gal, A. Pocheau, V. Croquette, Phys. Rev. Lett. **54**, 2501 (1985)
[5] E. Moses, V. Steinberg, Phys. Rev. Lett. **57**, 2018 (1986)
[6] E. Moses, V. Steinberg, Phys. Rev. **A43**, 707 (1991)
[7] P. Bigazzi, S. Ciliberto, V. Croquette, J. Phys. (France) **51**, 611 (1990)
[8] M. A. Dominguez-Lerma, G. Ahlers, and D. S. Cannell, Phys. Rev. **A52**, 6159 (1995)
[9] Ch. Jung, B. Huke, M. Lücke, Phys. Rev. Lett. **81**, 3651 (1998)
[10] B. Huke, M. Lücke, P. Büchel, Ch. Jung, J. Fluid Mech. **408**, 121 (2000)
[11] R. W. Walden, P. Kolodner, A. Passner, and C. M. Surko, Phys. Rev. Lett. **55**, 496 (1985)
[12] D. Bensimon, P. Kolodner, C. M. Surko, H. Williams, V. Croquette, J. Fluid Mech. **217**, 441 (1990)
[13] P. Kolodner, Phys. Rev. A **46**, 6452 (1992)
[14] P. Kolodner, Phys. Rev. E **50**, 2731 (1994)
[15] D. Jung, M. Lücke, Phys. Rev. Lett. **89**, 054502 (2002)
[16] D. Jung, P. Matura, M. Lücke, Eur. Phys. J. E. **15**, 293 (2004)
[17] P. Matura, D. Jung, M. Lücke, Phys. Rev. Lett. **92**, 254501 (2004)
[18] D. Jung, M. Lücke, Phys. Rev. E **72**, 026307 (2005)
[19] R. Cerbino, A. Vailati, and M. Giglio, Phys. Rev. E **66**, 055301 (2002); R. Cerbino, S.Mazzoni, A. Vailati, and M. Giglio, Phys. Rev. Lett. **94**, 064501 (2005).
[20] E. Blums, S. Odenbach, A. Mezulis, M. Maiorov, Phys. Fluids **10**, 2155 (1998)
[21] A. Ryskin, H.-W. Müller, H. Pleiner, Phys. Rev. E **67**, 046302 (2003)
[22] A. Ryskin, H. Pleiner, Phys. Rev. E **71**, 056303 (2005)

[23] W. Hort, S. Linz, M. Lücke, Phys. Rev. A **45**, 3737 (1992)
[24] K. I. Morozov, 'On the theory of the Soret effect in colloids'. In: *Thermal Nonequilibrium Phenomena in Fluid Mixtures*, ed. by W. Köhler and S. Wiegand. Lecture Notes in Physics **584**, 38. (Springer, Berlin, Heidelberg 2002)
[25] S. Chandrasekhar, *Hydrodynamic and hydromagnetic stability*, Appendix V (Dover, 1981)
[26] The critical wave number is $k_c^0 = 3.1163$. The value $k_c^0 = 3.117$ that can be found in many publications, e.g., in [25] seems to go back to the work of [46].
[27] The stability range, i. e., the so-called Busse balloon of these 2D convection structures has been evaluated for pure fluids [28] and for binary molecular mixtures [10]. We mention that in experiments defects appear in this roll pattern that are generated, e. g., by the preference of the rolls to be oriented normally to the side walls of the container. The lateral flows that are driven by the defected, curved rolls can then lead to complex defect and phase dynamics [29]. This, however, can easily be avoided by using narrow, annularly closed convection channels. They enforce the rolls to be oriented radially, i. e., practically parallel to each other in narrow annular channels with large radii.
[28] F. H. Busse, Rep. Prog. Phys. **41**, 1929 (1978).
[29] E. Bodenschatz, W. Pesch, and G. Ahlers, Annu. Rev. Fluid Mech. **32**, 709 (2000).
[30] St. Hollinger and M. Lücke, Phys. Rev. E **52**, 642 (1995).
[31] O. Lhost and J. K. Platten, Phys. Rev. A **40**, 6415 (1989).
[32] Chr. Jung, PhD thesis, Universität des Saarlandes (1997)
[33] St. Hollinger, M. Lücke, H. W. Müller, Phys. Rev. E **57**, 4250 (1998)
[34] T. Clune and E. Knobloch, Phys. Rev. A **44**, 8084 (1991)
[35] St. Odenbach, private communication
[36] B. I. Winkler and P. Kolodner, *Measurements of the concentration field in nonlinear travelling-wave convection* J. Fluid Mech. **240**, 31 (1992)
[37] H. Touiri, J. K. Platten, and G. Chavepeyer, Eur. J. Mech. B **15**, 241 (1996)
[38] E. Kaplan, E. Kuznetsov, and V. Steinberg, Phys. Rev. E **50**, 3712 (1994)
[39] C. M. Surko, D. R. Ohlsen, S. Y. Yamamoto, and P. Kolodner, Phys. Rev. A **43**, R7101 (1991)
[40] C. M. Aegerter and C. M. Surko, Phys. Rev. E **63**, 46301 (2001)
[41] L. Ning, Y. Harada, and H. Yahata, Prog. Theor. Phys. **98**, 551 (1997).
[42] O. Batiste, E. Knobloch, I. Mercader, and M. Net, Phys. Rev. E **65**, 016303 (2001)
[43] E. Moses, J. Fineberg, and V. Steinberg, Phys. Rev. A **35**, R2757 (1987); R. Heinrichs, G. Ahlers, D. S. Cannell, *ibid.* **35**, R2761 (1987)
[44] K. E. Anderson and R. P. Behringer, Phys. Lett. A **145**, 323 (1990); K. E. Anderson and R. P. Behringer, Physica D **51**, 444 (1991)
[45] St. Hollinger, P. Büchel, M. Lücke, Phys. Rev. Lett. **78**, 235 (1997)
[46] W. H. Reid and D. L. Harris, Phys. Fluids **1**, 102 (1958)